Journal of Molecular Graphics and Modelling 49 (2014) 91–98

Contents lists available at ScienceDirect

Journal of Molecular Graphics and Modelling

journal homepage: www.elsevier.com/locate/JMGM

Toward activated homology models of the human M_1 muscarinic acetylcholine receptor

Sek Peng Chin [a], Michael J.C. Buckle [a,*], David K. Chalmers [b], Elizabeth Yuriev [b], Stephen W. Doughty [c,**]

[a] Department of Pharmacy, Faculty of Medicine, University of Malaya, 50603 Kuala Lumpur, Malaysia
[b] Medicinal Chemistry, Monash Institute of Pharmaceutical Sciences, Monash University (Parkville Campus), 381 Royal Parade, Parkville, Victoria 3052, Australia
[c] The School of Pharmacy, University of Nottingham Malaysia Campus, Jalan Broga, 43500 Semenyih, Selangor, Malaysia

ARTICLE INFO

Article history:
Received 14 August 2013
Received in revised form 14 February 2014
Accepted 17 February 2014
Available online 25 February 2014

Keywords:
G protein-coupled receptor
Homology modeling
Docking
Virtual screening
Activated structure

ABSTRACT

Structure-based virtual screening offers a good opportunity for the discovery of selective M_1 muscarinic acetylcholine receptor (mAChR) agonists for the treatment of Alzheimer's disease. However, no 3-D structure of an M_1 mAChR is yet available and the homology models that have been previously reported are only able to identify antagonists in virtual screening experiments. In this study, we generated a homology model of the human M_1 mAChR, based on the crystal structure of an M_3 mAChR as the template. This initial model was modified, using the agonist-bound crystal structure of a β_2-adrenergic receptor as a guide, to give two possible activated structures. The T192 side chain was adjusted in both structures and one of the structures also had the whole of transmembrane (TM) 5 rotated and tilted toward the inner channel of the transmembrane region. The binding sites of all three structures were then refined by induced-fit docking (IFD) with acetylcholine. Virtual screening experiments showed that all three refined models could efficiently differentiate agonists from decoy molecules, with the TM5-modified models also giving good agonist/antagonist selectivity. The whole range of agonists and antagonists was observed to bind within the orthosteric site of the structure obtained by IFD refinement alone, implying that it has inactive state character. In contrast, the two TM5-modified structures were unable to accommodate the antagonists, supporting the proposition that they possess activated state character.

1. Introduction

The M_1 muscarinic acetylcholine receptor (mAChR) is a family A/class 1 G protein-coupled receptor (GPCR). All GPCRs share the same overall structural topology of seven transmembrane (TM) helices connected by alternating intracellular and extracellular loops (ICLs and ECLs, respectively). To date, five muscarinic receptor subtypes have been identified, which show an extraordinarily high degree of sequence similarity across different species and subtypes. The "odd-numbered" stimulatory muscarinic receptors (M_1, M_3, M_5) couple through the subunits of the $G_{q/11}$ family to activate phospholipase C, resulting in the release of the second messenger inositol 1,4,5-trisphosphate and the subsequent mobilization of intracellular calcium, whereas the "even-numbered" inhibitory muscarinic receptors (M_2, M_4) inhibit adenylyl cyclase activity via activation of the $G_{i/o}$ class of G protein, reducing intracellular levels of cAMP [1]. An important molecular distinction between the different muscarinic receptor subtypes is the sequence divergence in intracellular loop 3 (ICL3) between the $M_1/M_3/M_5$ sequences and the M_2/M_4 sequences, which probably determines the coupling preferences of these two groups [2].

The use of selective M_1 mAChR agonists has promising potential for the treatment of Alzheimer's disease since they are not only capable of restoring cognitive functions but can also act as disease modifiers through promotion of the non-amyloidogenic processing of amyloid precursor protein and inhibition of tau hyperphosphorylation [3–5]. However, to date, such agents have not yet been used clinically due to a lack of subtype selectivity and/or intrinsic activity. To assist the design of new M_1 mAChR agonists, a reliable three-dimensional (3-D) structure of the receptor is required.

* Corresponding author. Tel.: +60 3 79676658; fax: +60 3 79674964.
** Corresponding author. Tel.: +60 3 89248200; fax: +60 3 89248013.
E-mail addresses: buckle@um.edu.my (M.J.C. Buckle), stephen.doughty@nottingham.edu.my (S.W. Doughty).

http://dx.doi.org/10.1016/j.jmgm.2014.02.002
1093-3263/

In the absence of an experimental high-resolution structure, 3-D models can be obtained by homology modeling. Previously, M_1 mAChR homology models have been constructed based on crystal structures of either bovine rhodopsin [6–11] or the β_2-adrenergic receptor [12,13]. Recently, crystal structures of M_2 and M_3 mAChRs have been solved [14,15]. Since these receptors are expected to bear closer structural resemblance to the M_1 mAChR than bovine rhodopsin or the β_2-adrenergic receptor due to their high degrees of sequence similarity, they provide an opportunity to develop an improved 3-D models of the M_1 mAChR. Although an M_1 mAChR model has already been generated based on the crystal structure of the human M_2 mAChR complexed with an antagonist (PDB code: 3UON) [16], similar to previous M_1 mAChR models [6,8,12,13], it was only reported to be able to identify antagonists in virtual screening experiments, probably due to the fact that these models were all based on inactive structures.

In this study, as part of our continuing efforts to produce competent models of GPCRs [17], we have constructed models of the human M_1 mAChR based on the crystal structure of the rat M_3 mAChR (PDB code: 4DAJ), modified using the agonist-bound crystal structure of a β_2-adrenergic receptor (PDB code: 3SN6) [18] as a guide, and refined by induced-fit docking (IFD) with acetylcholine (ACh). The abilities of these models to differentiate agonists from decoy molecules and antagonists were then investigated. The binding poses of docked agonists and antagonists were also examined. To the best of our knowledge, these are the first reported M_1 receptor models, which are able to identify agonists effectively, and thus can be used as targets for structure-based discovery of novel compounds for the treatment of Alzheimer's disease.

2. Methodology

All-atom molecular models were generated and IFD, docking and enrichment studies were performed using Schrödinger suite 2011 (Schrödinger LLC, New York, USA) with default settings and parameters, unless stated otherwise [19–21]. Visual inspections were carried out with the aid of Maestro v9.2 (Schrödinger LLC), and Discovery Studio (DS) Visualizer v3.1 (Accelrys Inc., San Diego, CA, USA). Binding mode analyses were performed using the scripts within Maestro and DS Visualizer 2-D interaction diagrams. VMD [22] and PyMOL v1.3 (Schrödinger LLC) were used to produce 3-D figures. Structural validation of models was carried out using PROCHECK [23] and WHATCHECK [24]. For ease of comparison and standardization, GPCR residues are labeled using both their amino acid sequence number and Ballesteros–Weinstein nomenclature, as a superscript extension [25].

2.1. Homology modeling

The sequence of the human M_1 mAChR (accession number: P11229) was retrieved from the Swiss-Prot sequence database [26]. Guided alignment of the human M_1 receptor sequence and that obtained from the structure of the rat M_3 mAChR complexed with an inverse agonist (PDB code: 4DAJ), was carried out using the Expresso structural sequence alignment program [27], which takes structural aspects into account during the alignment process. The alignment was based on the classic GPCR structural fingerprints (asparagine in TM1, aspartic acid in TM2, the "DRY" motif in TM3, tryptophan in TM4 and the conserved proline residues in TM5, TM6, and TM7). The alignment was inspected manually to avoid gaps in the TM domains and to enforce alignment of the highly conserved structural fingerprints of the class A GPCRs, including the conserved disulfide bridge. The Expresso score of the alignment was 99, suggesting a very good and reliable alignment (score > 50). ESPript [28] was used to display the final sequence alignment (see Supporting Information Fig. S1). The M_1 and M_3 receptor sequences were found to share 53% sequence identity overall, with the seven TM domains sharing 79% sequence identity. In contrast, following a similar alignment of the human M_1 mAChR receptor sequence and that obtained from the crystal structure of the human M_2 mAChR complexed with an antagonist (PDB code: 3UON), this pair of sequences was found to share a lower sequence identity (45% overall, 69% for the seven TM domains). For this reason and also due to the fact that the M_3 receptor, like the M_1 receptor, is an "odd-numbered" stimulatory muscarinic receptor and so has greater functional similarity to the M_1 receptor, the M_3 receptor structure was used as the template for homology modeling.

Following the sequence alignment, a crude homology model of the M_1 receptor was constructed and optimized using Prime v3.0 (Schrödinger LLC). The orientations of the amino acids in the putative binding pocket, which are completely conserved across mAChRs, were frozen and retained in the crude model. ECLs and ICLs connecting the TM domains were modeled according to the template structure except ICL3, which was excluded from the modeling.

2.2. Binding site refinement

Since the shape of the binding pocket of the template is likely to have been influenced by the bound inverse agonist (tiotropium), binding site refinement was carried out by constructing a cubic box of 28 Å × 28 Å × 28 Å, centered on the centroid of selected known orthosteric site residues ($D105^{3.32}$, $Y106^{3.33}$, $W157^{4.57}$, $T189^{5.39}$, $T192^{5.42}$, $W378^{6.48}$, $Y381^{6.51}$, $Y404^{7.39}$ and $Y408^{7.43}$) of the M_1 mAChR suggested by site-directed mutagenesis (SDM) studies [10,29–33], followed by IFD of the endogenous muscarinic receptor agonist (ACh) using Glide v5.7 (Schrödinger LLC) and side chain refinement using Prime v3.0. The IFD protocol began with a constrained minimization of the receptor structure, followed by initial Glide docking of ACh using a softened potential, to allow more poses of the ligand to be generated and collected. One round of side-chain refinement was then carried out for the residues found within 5 Å of the ligand, followed by minimization of each ligand–receptor complex. Finally, the ligand was re-docked into the induced-fit receptor structure, without softened potential and the binding energy or IFD score was obtained. After multiple iterations of docking and binding site refinement, an initial set of models was chosen on the basis of showing the expected ligand–receptor interactions. The resulting ligand–receptor conformations were inspected visually to ensure that the quaternary amine group of the docked ACh was directed toward the conserved $D105^{3.32}$ and the side chains of the orthosteric site residues were facing inwards toward the inner channel of the TM region. The best model (henceforth referred to as model 1) was then selected on the basis of enrichment study results.

2.3. Generation of activated structures

To generate an activated M_1 mAChR model, the best IFD-refined model (model 1), was superimposed on the activated β_2-adrenergic receptor structure (PDB code: 3SN6) and, as depicted in Fig. 1, TM3, TM5 and TM6 were shifted laterally with reference to the β_2-adrenergic receptor structure using the GPCR Helix Manipulator module in Maestro v9.2, following the precedent set for the activation of a β_2-adrenergic receptor [34]. The side chain rotamer of $T192^{5.42}$ was then adjusted and the resulting structure subjected to IFD with ACh to produce model 1A1. Further modifications on model 1A1 were carried out whereby TM5 was rotated clockwise and tilted toward the inner channel of the TM region and the resulting structure was again subjected to IFD to give model 1A2. The

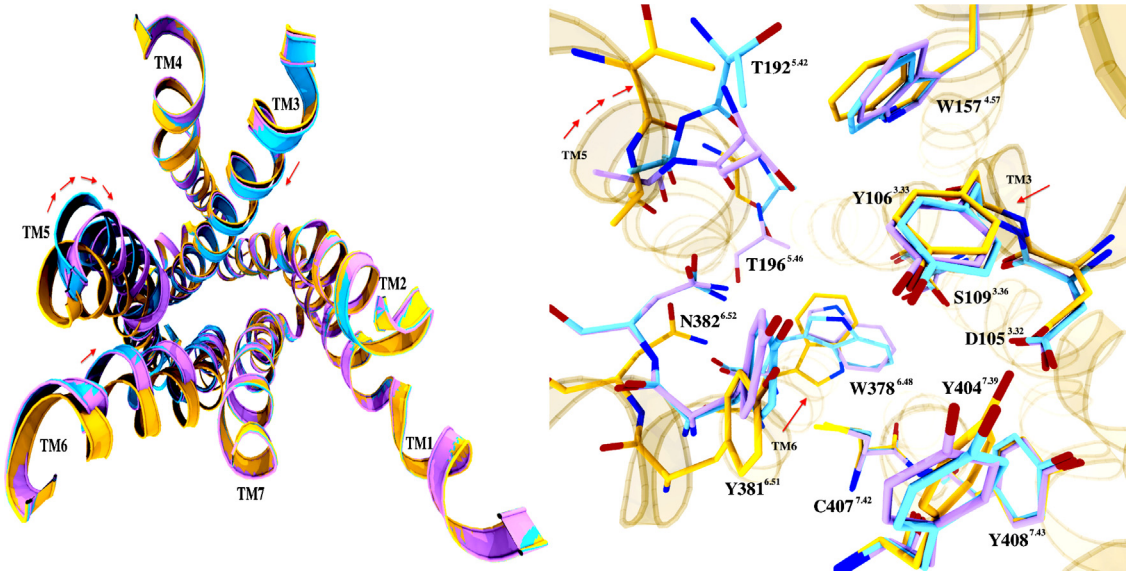

Fig. 1. Superposition of models 1 (yellow), 1A1 (blue) and 1A2 (purple) with the important interacting side chain orientations for each of the models shown in stick representation. Loops are not shown for the purpose of clarity.

models reported were selected on the basis of enrichment study results.

2.4. Enrichment and docking studies

Enrichment studies were carried out to test the ability of the refined models to differentiate agonists from decoys. A set of 51 reported agonists (see Supporting Information Fig. S2) for the M_1 mAChR was retrieved from GLIDA, the GPCR-ligand database [35] and IUPHAR-DB [36] and their 3-D coordinates were obtained from PubChem [37]. Two sets of decoys were used in these studies. The Schrödinger set (Set I), containing 1000 drug-like ligands, which were selected randomly from a library of one million compounds, was obtained from www.schrodinger.com [19,20], whereas the property-matched set (Set II), containing 1499 decoy molecules, was derived from the ZINC database [38], based on having properties which were matched to those of each of the agonists, i.e. in numbers of heavy atoms (same as parent ± 3), H-bond donors (same as parent ± 1), H-bond acceptors (same as parent ± 2), rotatable bonds (same as parent ± 2), number of rings (same as parent ± 1), and with a Tanimoto similarity score <0.5 with respect to each other and the parents (to ensure topological diversity). The molecular properties and Tanimoto scores of the agonists and decoys were calculated using Discovery Studio v3.1 (Accelrys Inc.) with predefined parameters. Although neither decoy set was substantially biased in terms of polarity (log P, numbers of donors and acceptors) or aromaticity (numbers of aromatic rings), compared with the agonists, Set II was more closely matched (see Supporting Information Table S1). In contrast to Set I, which was not specifically chosen to match the agonists, Set II can be considered as efficient challengers for the agonists (having similar molecular properties without being chemically similar). Ligands were prepared using LigPrep v2.5 (Schrödinger LLC) to assign appropriate protonation states, generate tautomers and optimize geometry prior to docking calculations. The decoy sets enriched with the 51 agonists was flexibly docked into the M_1 receptor models using Glide v5.7 [19,20] and the bound poses were ranked by GlideScore. The grid box settings were the same as those used for IFD, accommodating ligands with a length of 20 Å or less and with a default inner box of 10 Å on each side. Glide Standard Precision scoring functions were used and one pose per ligand was collected for analysis. Enrichment factors (EF) were calculated at 2%, 5% and 10% of the total library screened, using the following equation:

$$\mathrm{EF} = \frac{\mathrm{Hits}_{\mathrm{sampled}}/N_{\mathrm{sampled}}}{\mathrm{Hits}_{\mathrm{total}}/N_{\mathrm{total}}}$$

where Hits is the number of actives and N is the number of compounds (actives and decoys).

Receiver operating characteristic (ROC) curves were plotted as the true positive rate against the false positive rate [39]. The Boltzmann-enhanced discrimination of receiver operating characteristic (BEDROC) [40] and ROC area under the curve (AUC) values were calculated to measure the early recognition performance and the overall predictive performance, respectively, of each model.

To access the abilities of the models to differentiate agonists from antagonists, additional docking studies were carried out on a set of 50 reported antagonists (see Supporting Information Fig. S3) which were retrieved, downloaded and prepared as described earlier for the agonist set. The Mann–Whitney U test was used to compare the Gscore values obtained from docking studies on agonists and antagonists, with $p < 0.01$ being considered to be significant.

3. Results and discussion

3.1. Model validation

All the generated models preserved the specific signature features of GPCRs and showed similar structural features to the M_3 mAChR template (PDB code: 4DAJ). Thus superposition of the generated models on the M_3 mAChR template, the agonist-bound β_2-adrenergic structure and various other solved GPCR crystal structures showed good overlap, with RMSD values in the range 0.1–2.5 Å (see Supporting Information Fig. S4 and Table S2). Models 1A1 and 1A2, which were obtained by modification using the agonist-bound crystal structure of a β_2-adrenergic receptor (PDB code: 3SN6) as a guide, followed by binding site refinement using IFD, possessed smaller binding pockets than model 1 (the best model obtained from IFD refinement alone) (Fig. 1). In addition to the contraction of the binding cavity, the other prominent feature observed in agonist-bound structures is the outward movement of

TM6 [41]. However, models 1A1 and 1A2 did not reproduce this feature due to the nature of the induced-fit methodology used.

The chosen M_1 receptor homology models were subjected to extensive validation analysis using PROCHECK [23] and WHATCHECK [24]. The results indicated that the models are reasonably good structurally with all the residues contributing substantially to ligand binding being found in the allowed regions of the Ramachandran plot (Supporting Information Table S3). Model 1 had no residues in the disallowed region and had the largest number of residues in the most favored regions. Model 1A1 had two residues (T215$^{5.65}$ and T366$^{6.36}$) in the disallowed region which are located near the end of TM5 and the beginning of TM6, where ICL3 was truncated. Model 1A2 had one residue (T366$^{6.36}$) in the disallowed region. Neither of these residues is in the vicinity of the binding cavity of the receptor. All the models demonstrated WHATCHECK scores better or comparable with the template with no severe errors and all *Z*-scores being within the normal range, except for backbone conformation and inside/outside distribution (see Supporting Information Table S4). The reason for the latter observation may simply be that TM helices are not very often seen in the database of solved protein structures and the database is not optimized for membrane proteins. Overall, the scores indicated that all the models have no discernable shortcomings structurally.

3.2. Enrichment and docking studies

The three refined models were found to give considerably better enrichment for 51 reported agonists than the crude model (Fig. 2 and Table 1), yielding AUC values in excess of 0.70, except for model 1 in the case the Schrödinger decoy set (Set I), suggesting that they are all able to differentiate between agonists and decoys moderately accurately [42]. Although both sets of decoys produced quite similar enrichment data, we chose to analyze the results obtained from using Set II, as the better match of the molecular properties between the decoys and the agonists, compared to Set I, is expected to give unbiased results and a good reflection of the actual performance of the models. Model 1A1 recorded the highest EF 2% and BEDROC value, which is considered to be the best indicator of the ability of a model to give early recognition of actives [40]. Model 1A2 failed to bind 24% (12/51) of the larger agonists, including NCC 11-1585, NCC 11-1607 and pentylthio-TZTP (see Supporting Information Fig. S2), which are described as full agonists in the IUPHAR database. This suggests that the smaller and tighter binding cavity of model 1A2 is unable to accommodate bulkier molecules.

Docking of 50 reported antagonists resulted in 100% and 96% (48) of them being able to bind to models 1 and 1A1, respectively, whereas model 1A2 was only able to accommodate 28% (14) of the antagonists. However, it was found that the Gscore values for those antagonists that bound to model 1A1 tended to be significantly lower ($p < 0.01$) than for the 51 agonists. A similar trend was observed for antagonist and agonist docking to model 1A2. Thus, on the basis of Gscore values, both models 1A1 and 1A2 exhibited a marked selectivity for agonists over antagonists, with excellent EF2% (19 and 25, respectively) and BEDROC values (0.987 and 0.997, respectively). Conversely, in the case of model 1,

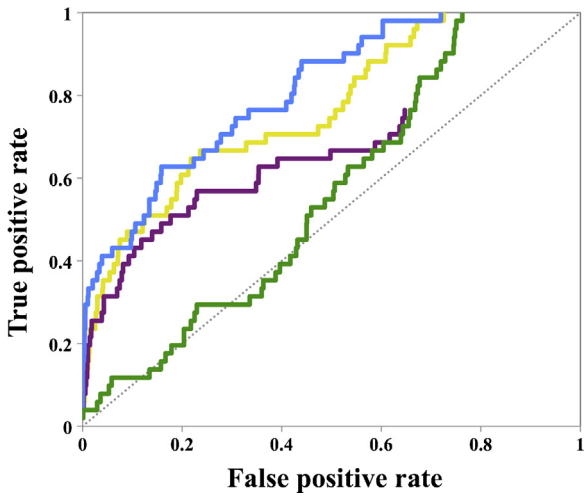

Fig. 2. Receiver operating characteristic (ROC) agonist enrichment plots using the property-matched decoy set (Set II) for the different homology models: green, crude model; yellow, model 1; blue, model 1A1; purple, model 1A2. (For interpretation of the references to color in this legend, the reader is referred to the web version of the article.)

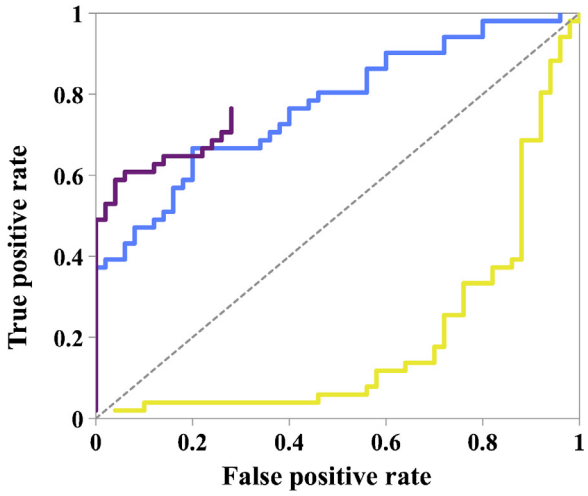

Fig. 3. Receiver operating characteristic (ROC) plots showing the agonist/antagonist selectivity for the different homology models: yellow, model 1; blue, model 1A1; purple, model 1A2. (For interpretation of the references to color in this legend, the reader is referred to the web version of the article.)

Table 1
Analysis of data from enrichment studies for the crude and refined models.

Decoy set/model			Crude	1	1A1	1A2
Set I (Schrödinger)	BEDROC		0.102	0.244	0.480	0.526
	AUC		0.34	0.67	0.75	0.72[a]
	EF	2%	2.0	5.9	17	19
		5%	1.6	3.5	7.8	9.4
		10%	0.98	2.9	4.1	5.1
Set II (property-matched)	BEDROC		0.097	0.355	0.440	0.324
	AUC		0.56	0.76	0.80	0.77[a]
	EF	2%	2.0	12	17	13
		5%	1.6	7.1	8.2	6.3
		10%	1.2	4.7	4.7	4.1

[a] Calculated based on the number of agonists and decoys that successfully bound to model 1A2.

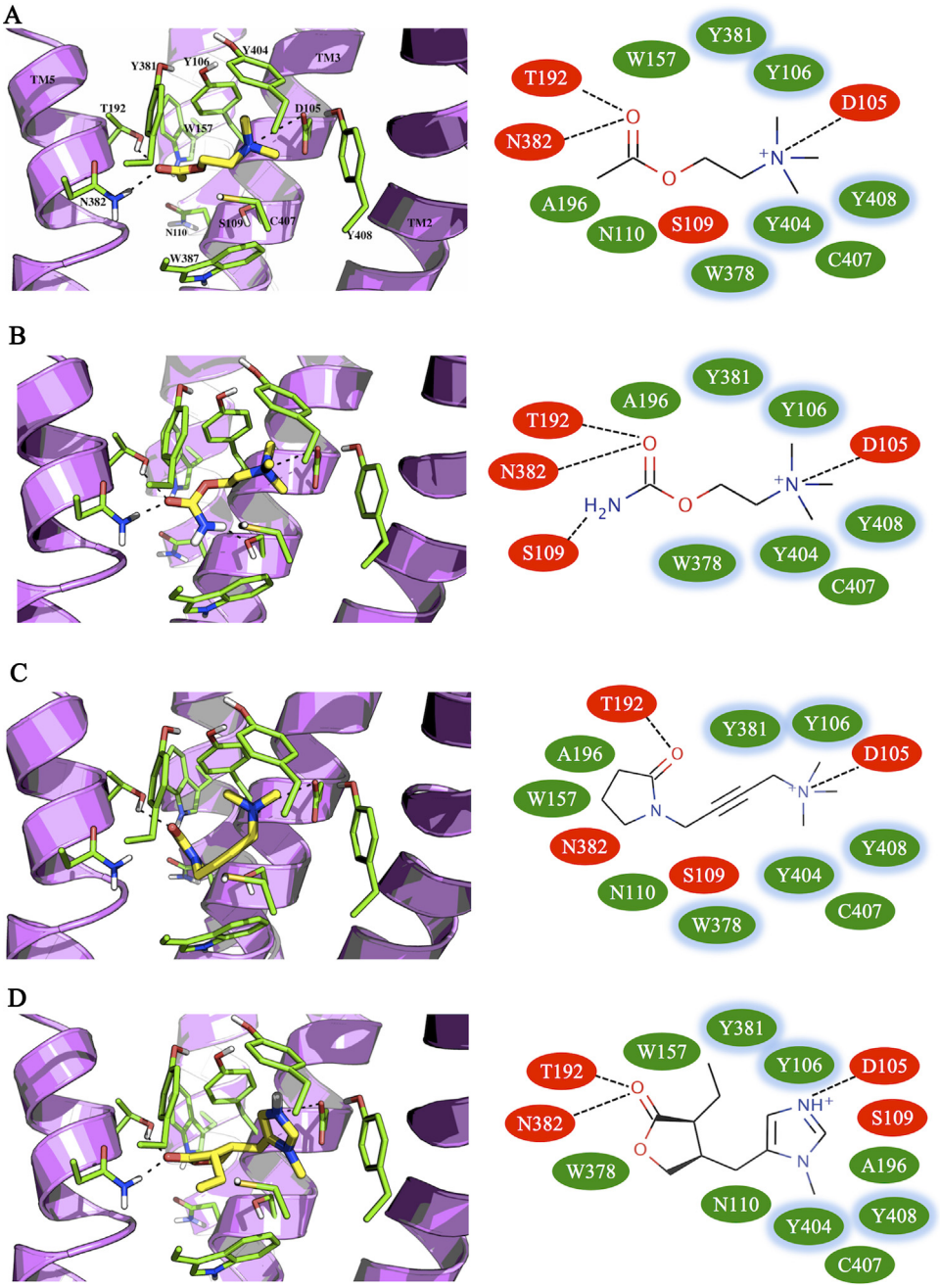

Fig. 4. The binding modes of representative agonists with model 1A2. (A) ACh, (B) carbachol, (C) oxotremorine-M, and (D) pilocarpine. The important interacting residues are shown in stick representation and labeled. For the purpose of clarity, ECLs, ICLs, TM1, TM6, and TM7 are not shown. Residues involved in hydrogen bonding, charged, or polar interactions are shaded in red. Residues involved in van der Waals interactions are shaded in green. Residues involved in pi interactions are shown with a blue ring. (For interpretation of the references to color in this legend, the reader is referred to the web version of the article.)

the Gscore values for bound antagonists tended to be significantly higher ($p < 0.01$) than for bound agonists, resulting in a reversal of the agonist/antagonist selectivity. These observations are clearly illustrated by the agonist/antagonist selectivity ROC plots shown in Fig. 3. Taken together, these results suggest that models 1A1 and 1A2 possess activated state character, whereas model 1 has inactive state character.

3.3. Analysis of ligand binding modes

Analysis of the antagonist binding locations for each of the models revealed that, whereas 88% (44/50) of the antagonists docked to the orthosteric site of model 1, in the activated models 1A1 and 1A2, nearly all of the antagonists (46/48 and 13/14, respectively) did not dock within the orthosteric site but instead were found at a site adjacent to the orthosteric site, toward the extracellular surface of the receptor and some distance away from the conserved D105$^{3.32}$ residue (see Supporting Information Fig. S5). This observation is consistent with the proposal that antagonists have low affinity for activated receptor conformations [43] and in fact may not fit within the smaller, activated orthosteric site. Furthermore, suboptimal binding at this external site may account for the lower Gscore values obtained for antagonists bound to the activated models. Interestingly, the location of this site seems to closely correspond to that of the allosteric site that has been identified in molecular dynamics (MD) simulation studies of the binding

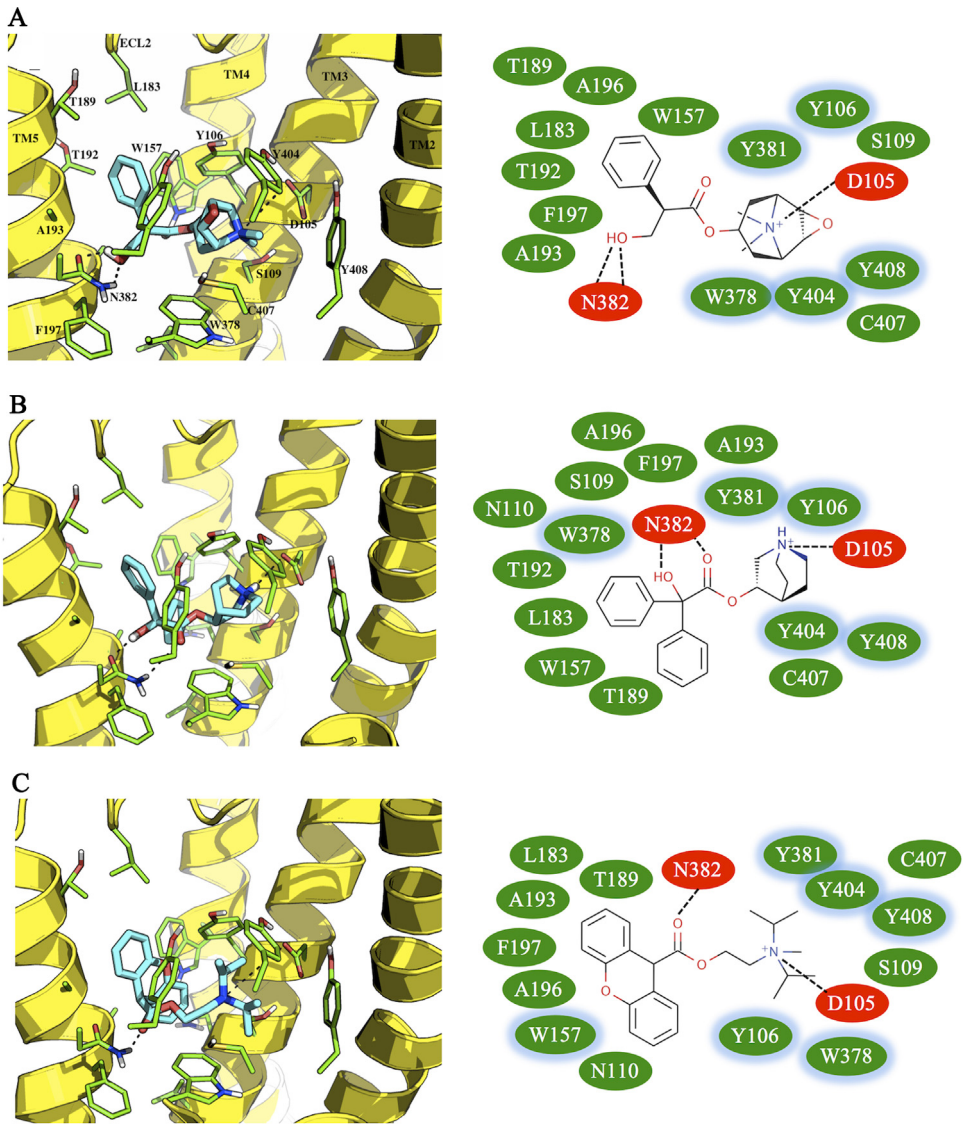

Fig. 5. The binding modes of representative antagonists with model 1. (A) NMS, (B) QNB, and (C) propantheline. The important interacting residues are shown in stick representation and labeled. For the purpose of clarity, ECLs, ICLs, TM1, TM6, and TM7 are not shown. Residues involved in hydrogen bonding, charged, or polar interactions are shaded in red. Residues involved in van der Waals interactions are shaded in green. Residues involved in pi interactions are shown with a blue ring. (For interpretation of the references to color in this legend, the reader is referred to the web version of the article.)

of the inverse agonist, tiotropium, to M_2 and M_3 receptor models [15], derived from their respective crystal structures. The fact that, in general, both the agonists and the antagonists bind within the orthosteric site of model 1, whereas only the agonists bind to this site in models 1A1 and 1A2, supports the proposition that model 1 resembles an inactive state, while models 1A1 and 1A2 more closely represent an activated state.

Of the two activated models, model 1A2 more strongly discriminates between agonists and antagonists. When we examined the binding orientation of agonists within this model we found that that 80% conformed to the expected binding modes, making interactions with the key residues identified by SDM experiments [10,29–33]. This observation demonstrates that the models are not strongly biased toward the structure of the agonist (ACh) that was used in the binding site refinement and are capable of correctly predicting the binding interactions of structurally diverse ligands. Similar results were also obtained for refined models 1 and 1A1.

Fig. 4 shows the interaction patterns for the representative agonists, ACh, carbachol, oxotremorine-M and pilocarpine docked with model 1A2. All the ligands form a polar charged interaction with the conserved D105$^{3.32}$ and cation–pi interactions with aromatic residues Y106$^{3.33}$, W378$^{6.48}$, Y381$^{6.51}$, Y404$^{7.39}$ and Y408$^{7.43}$ through their positively-charged head groups, and hydrophobic interactions with the latter set of residues and others, including A196$^{5.46}$ and C407$^{7.42}$ (see Supporting Information Table S5). The interactions within model 1A2 are in particularly close agreement with the SDM data, with hydrogen bonding between both T192$^{5.42}$ and N382$^{6.52}$ and the carbonyl oxygen atom in the agonist tail groups [44]. Furthermore, the fact that, in all three models, Y381$^{6.51}$ is involved in pi–cation interactions with ACh suggests that the models contain important features of the activated state [30].

The binding model of the representative antagonists, *N*-methylscopolamine (NMS), (−)-3-quinuclidinyl benzilate (QNB) and propantheline is shown in Fig. 5. These compounds were found to bind to the orthosteric pocket in model 1 with the positively charged head groups interacting in a similar way to the agonists discussed above. The main differences were that the antagonists exhibited additional hydrophobic interactions with A193$^{5.43}$, while hydrogen bonding interactions were only observed with N382$^{6.52}$ and not with T192$^{5.42}$ (see Supporting Information Table S6). These

differences are also in good agreement with SDM experiments, in which mutations to these residues were observed to have greater effects on the binding of antagonists than that of agonists [31,44]. In the case of QNB, the docked binding mode reproduced that found in the crystal structure of its complex with the human M_2 receptor (PDB code: 3UON), in which both the carbonyl and hydroxyl groups were observed to hydrogen bond to the equivalent asparagine residue.

Superposition of all the ligands that successfully docked to the refined models, showed that the binding cavities for the agonists and antagonists overlap, but with the antagonist binding cavity extending toward the extracellular vestibule and ECL2 (see Supporting Information Fig. S6). Nevertheless, while the head groups for both agonists and antagonists were directed toward the conserved D105$^{3.32}$, the tail groups positioned themselves differently, confirming observations made in a previous study [10].

Structural interaction fingerprinting [45] was used to further investigate the binding of agonists and antagonists to models 1 and 1A2 (see Supporting Information Table S7). The interactions map was able to distinguish between the agonist and antagonist binding patterns and confirmed the importance of T192$^{5.42}$ and N382$^{6.52}$ in agonist and antagonist binding, respectively. Even though T192$^{5.42}$ was found within 4 Å of 76% of the docked antagonists, none of them established a hydrogen bond with this residue, in contrast with 18% of the agonists. On the other hand, almost half of the antagonists were found to form hydrogen bonds with N382$^{6.52}$, whereas this interaction does not seem to be mandatory for the agonists. Furthermore, A193$^{5.43}$ was completely absent from agonist binding in model 1A2 and relatively unimportant in model 1, but contributed hydrophobic interactions with almost all the antagonists. L183, which extends downward from ECL2 toward the binding cavity, was observed as part of the binding pocket for 84% of the antagonists but only 18% for the agonists, while another ECL2 residue, I180, was found to be involved in the binding of antagonists but was absent from agonist binding. These residues emphasize the role of ECL2 in ligand binding, especially for the relatively larger antagonists. Overall, the results show that the binding modes of agonists are clearly different to those of antagonists. This is in agreement with observations made on agonist-bound crystal structures of β_1- and β_2-adrenergic receptors [46,47].

4. Conclusion

GPCR models that can correctly identify active compounds and furthermore discriminate agonists from antagonists are important tools for rational drug design. Two main complementary approaches currently used for structure-based drug design against GPCRs are virtual screening and MD [48,49]. In the context of muscarinic acetylcholine receptors, recent MD simulations of M_2 and M_3 receptors have provided enlightening insights into the binding pathways of agonist and antagonist ligands and have demonstrated the influence of binding site volume on the selectivity profiles of ligands of varying size [15,50].

In this study, we have developed refined human M_1 mAChR homology models based on a crystal structure of an M_3 mAChR, which efficiently differentiate agonists from decoy molecules and exhibit high agonist/antagonist selectivity in docking studies. Model 1A2, in which the orientation of the T192$^{5.42}$ side chain was adjusted and the whole TM5 was rotated and tilted toward the inner channel of the TM region, gives the best prediction of the binding poses and interactions of small to medium-sized agonists, although agonists that are larger or bulkier are unable to dock into its relatively tight binding pocket. On the other hand, models 1 and 1A1 are both able to bind the whole range of agonists, with model 1A1 giving good selectivity for agonists over antagonists and model 1 showing a high preference for antagonists over agonists. Since a single GPCR model is unlikely to be sufficient to completely represent the range of 'ligandable' conformations, we propose the combined use of models of 1, 1A1 and 1A2 for structure-based virtual screening to identify potential M_1 mAChR agonists and differentiate them from antagonists. MD simulations are also required to investigate further the conformational changes that occur upon ligand binding and the factors that influence subtype selectivity.

Acknowledgements

This study was funded by grants from the Ministry of Science, Technology and Innovation, Malaysia (02-01-03-SF0149) and the University of Malaya (PS191-2009C). S.P. Chin was a recipient of a National Science Fellowship from the Ministry of Science, Technology and Innovation, Malaysia. We would also like to acknowledge computational resources provided by the Victorian Life Sciences Computational Infrastructure through grant VR0133.

Appendix A. Supplementary data

Supplementary data associated with this article can be found, in the online version, at http://dx.doi.org/10.1016/j.jmgm.2014.02.002.

References

[1] C.C. Felder, Muscarinic acetylcholine receptors: signal transduction through multiple effectors, FASEB J. 9 (1995) 619–625.
[2] J. Wess, Molecular basis of muscarinic acetylcholine receptor function, Trends Pharmacol. Sci. 14 (1993) 308–313.
[3] A. Fisher, Cholinergic treatments with emphasis on M1 muscarinic agonists, Neurotherapeutics 5 (2008) 433–442.
[4] C.J. Langmead, J. Watson, C. Reavill, Muscarinic acetylcholine receptors as CNS drug targets, Pharmacol. Therapeut. 117 (2008) 232–243.
[5] A.A. Davis, J.J. Fritz, J. Wess, J.J. Lah, A.I. Levey, Deletion of M1 muscarinic acetylcholine receptors increases amyloid pathology in vitro and in vivo, J. Neurosci. 30 (2010) 4190–4196.
[6] C. Bissantz, P. Bernard, M. Hibert, D. Rognan, Protein-based virtual screening of chemical databases. II. Are homology models of G-protein coupled receptors suitable targets? Protein Struct. Funct. Genet. 50 (2003) 5–25.
[7] E.C. Hulme, Z.L. Lu, J.W. Saldanha, M.S. Bee, Structure and activation of muscarinic acetylcholine receptors, Biochem. Soc. Trans. 31 (2003) 29–34.
[8] A. Evers, G. Hessler, H. Matter, T. Klabunde, Virtual screening of biogenic amine-binding G-protein coupled receptors: comparative evaluation of protein- and ligand-based virtual screening protocols, J. Med. Chem. 48 (2005) 5448–5465.
[9] J.Y.C. Peng, N. Vaidehi, S.E. Hall, W.A. Goddard, The predicted 3D structures of the human M1 muscarinic acetylcholine receptor with agonist or antagonist bound, ChemMedChem 1 (2006) 878–890.
[10] J.A. Goodwin, E.C. Hulme, C.J. Langmead, B.G. Tehan, Roof and floor of the muscarinic binding pocket: variations in the binding modes of orthosteric ligands, Mol. Pharmacol. 72 (2007) 1484–1496.
[11] L.M. Espinoza-Fonseca, A. Pedretti, G. Vistoli, Structure and dynamics of the full-length M_1 muscarinic acetylcholine receptor studied by molecular dynamics simulations, Arch. Biochem. Biophys. 469 (2008) 142–150.
[12] F.M. McRobb, B. Capuano, I.T. Crosby, D.K. Chalmers, E. Yuriev, Homology modeling and docking evaluation of aminergic G protein-coupled receptors, J. Chem. Inf. Model. 50 (2010) 626–637.
[13] T. Thomas, K.C. McLean, F.M. McRobb, D.T. Manallack, D.K. Chalmers, E. Yuriev, Homology modeling of human muscarinic acetylcholine receptors, J. Chem. Inf. Model. 54 (2014) 243–253.
[14] K. Haga, A.C. Kruse, H. Asada, T. Yurugi-Kobayashi, M. Shiroishi, C. Zhang, W.I. Weis, T. Okada, B.K. Kobilka, T. Haga, T. Kobayashi, Structure of the human M2 muscarinic acetylcholine receptor bound to an antagonist, Nature 482 (2012) 547–551.
[15] A.C. Kruse, J. Hu, A.C. Pan, D.H. Arlow, D.M. Rosenbaum, E. Rosemond, H.F. Green, T. Liu, P.S. Chae, R.O. Dror, D.E. Shaw, W.I. Weis, J. Wess, B.K. Kobilka, Structure and dynamics of the M3 muscarinic acetylcholine receptor, Nature 482 (2012) 552–556.
[16] B. Jójárt, A.M. Balint, S. Balint, B. Viskolcz, Homology modeling and validation of the human M1 muscarinic acetylcholine receptor, Mol. Inf. 31 (2012) 635–638.
[17] B.K. Yap, M.J.C. Buckle, S.W. Doughty, Homology modeling of the human 5-HT1A, 5-HT2A, D1, and D2 receptors: model refinement with molecular dynamics simulations and docking evaluation, J. Mol. Mod. 18 (2012) 3639–3655.
[18] S.G.F. Rasmussen, B.T. DeVree, Y. Zou, A.C. Kruse, K.Y. Chung, T.S. Kobilka, F.S. Thian, P.S. Chae, E. Pardon, D. Calinski, J.M. Mathiesen, S.T.A. Shah, J.A. Lyons, M. Caffrey, S.M. Gellman, J. Steyaert, G. Skiniotis, W.I. Weis, R.K. Sunahara, B.K.

Kobilka, Crystal structure of the β_2 adrenergic receptor–Gs protein complex, Nature 477 (2011) 549–555.
[19] R.A. Friesner, J.L. Banks, R.B. Murphy, T.A. Halgren, J.J. Klicic, D.T. Mainz, M.P. Repasky, E.H. Knoll, D.E. Shaw, M. Shelley, J.K. Perry, P. Francis, P.S. Shenkin, Glide: a new approach for rapid, accurate docking and scoring. 1. Method and assessment of docking accuracy, J. Med. Chem. 47 (2004) 1739–1749.
[20] T.A. Halgren, R.B. Murphy, R.A. Friesner, H.S. Beard, L.L. Frye, W.T. Pollard, J.L. Banks, Glide: a new approach for rapid, accurate docking and scoring. 2. Enrichment factors in database screening, J. Med. Chem. 47 (2004) 1750–1759.
[21] W. Sherman, T. Day, M.P. Jacobson, R.A. Friesner, R. Farid, Novel procedure for modeling ligand/receptor induced fit effects, J. Med. Chem. 49 (2006) 534–553.
[22] W. Humphrey, A. Dalke, K. Schulten, VMD – visual molecular dynamics, J. Mol. Graph. 14 (1996) 33–38.
[23] R.A. Laskowski, M.W. Macarthur, D.S. Moss, J.M. Thornton, PROCHECK: a program to check the stereochemical quality of protein structures, J. Appl. Cryst. 26 (1993) 283–291.
[24] R.W.W. Hooft, G. Vriend, C. Sander, E.E. Abola, Errors in protein structures, Nature 381 (1996) 272.
[25] J.A. Ballesteros, H. Weinstein, Integrated methods for the construction of three dimensional models and computational probing of structure–function relations in G protein coupled receptors, Methods Neurosci. 25 (1995) 366–428.
[26] B. Boeckmann, A. Bairoch, R. Apweiler, M.C. Blatter, A. Estreicher, E. Gasteiger, M.J. Martin, K. Michoud, C. O'Donovan, I. Phan, S. Pilbout, M. Schneider, The Swiss-Prot Protein Knowledgebase and its supplement TrEMBL in 2003, Nucleic Acids Res. 31 (2003) 365–370.
[27] F. Armougom, S. Moretti, O. Poirot, S. Audic, P. Dumas, B. Schaeli, V. Keduas, C. Notredame, Expresso: automatic incorporation of structural information in multiple sequence alignments using 3D-coffee, Nucleic Acids Res. 34 (2006) 604–608.
[28] P. Gouet, E. Courcelle, D.I. Stuart, F. Metoz, ESPript: multiple sequence alignments in PostScript, Bioinformatics 15 (1999) 305–308.
[29] Z.L. Lu, E.C. Hulme, The functional topography of transmembrane domain 3 of the M1 muscarinic acetylcholine receptor, revealed by scanning mutagenesis, J. Biol. Chem. 274 (1999) 7309–7315.
[30] S.D.C. Ward, C.A.M. Curtis, E.C. Hulme, Alanine-scanning mutagenesis of transmembrane domain 6 of the M1 muscarinic acetylcholine receptor suggests that Tyr381 plays key roles in receptor function, Mol. Pharmacol. 56 (1999) 1031–1041.
[31] K. Allman, K.M. Page, C.A.M. Curtis, E.C. Hulme, Scanning mutagenesis identifies amino acid side chains in transmembrane domain 5 of the M1 muscarinic receptor that participate in binding the acetyl methyl group of acetylcholine, Mol. Pharmacol. 58 (2000) 175–184.
[32] Z.L. Lu, J.W. Saldanha, E.C. Hulme, Transmembrane domains 4 and 7 of the M1 muscarinic acetylcholine receptor are critical for ligand binding and the receptor activation switch, J. Biol. Chem. 276 (2001) 34098–34104.
[33] T.A. Spalding, J.N. Ma, T.R. Ott, M. Friberg, A. Bajpai, S.R. Bradley, R.E. Davis, M.R. Brann, E.S. Burstein, Structural requirements of transmembrane domain 3 for activation by the M1 muscarinic receptor agonists AC-42, AC-260584, clozapine, and N-desmethylclozapine: evidence for three distinct modes of receptor activation, Mol. Pharmacol. 70 (2006) 1974–1983.
[34] S. Vilar, J. Karpiak, B. Berk, S. Costanzi, In silico analysis of the binding of agonists and blockers to the β_2-adrenergic receptor, J. Mol. Graph. Model. 29 (2011) 809–817.
[35] Y. Okuno, A. Tamon, H. Yabuuchi, S. Niijima, Y. Minowa, K. Tonomura, R. Kunimoto, C.G.L.I.D.A. Feng, GPCR ligand database for chemical genomics drug discovery database and tools update, Nucleic Acids Res. 36 (2008) D907–D912.
[36] J.L. Sharman, C.P. Mpamhanga, M. Spedding, P. Germain, B. Staels, C. Dacquet, V. Laudet, A.J. Harmar, NC-IUPHAR. IUPHAR-DB: new receptors and tools for easy searching and visualization of pharmacological data, Nucleic Acids Res. 39 (2011) D534–D538.
[37] E. Bolton, Y. Wang, P.A. Thiessen, S.H. Bryant, PubChem. Integrated Platform of Small Molecules and Biological Activities. Annual Reports in Computational Chemistry, vol. 4, American Chemical Society, Washington, DC, 2008, pp. 217–241 (Chapter 12).
[38] J.J. Irwin, T. Sterling, M.M. Mysinger, E.S. Bolstad, R.G. Coleman, ZINC: a free tool to discover chemistry for biology, J. Chem. Inf. Model. 52 (2012) 1757–1768.
[39] N. Triballeau, F. Acher, I. Brabet, J.P. Pin, H.O. Bertrand, Virtual screening workflow development guided by the receiver operating characteristic curve approach. Application to high-throughput docking on metabotropic glutamate receptor subtype 4, J. Med. Chem. 48 (2005) 2534–2547.
[40] J.F. Truchon, C.I. Bayly, Evaluating virtual screening methods: good and bad metrics for the early recognition problem, J. Chem. Inf. Model. 47 (2007) 488–508.
[41] G. Lebon, T. Warne, C.G. Tate, Agonist-bound structures of G protein-coupled receptors, Curr. Opin. Struct. Biol. 22 (2012) 482–490.
[42] J.A. Swets, Measuring the accuracy of diagnostic systems, Science 240 (1988) 1285–1293.
[43] T. Kenakin, Principles: receptor theory in pharmacology, Trends Pharm. Sci. 25 (2004) 186–192.
[44] X.P. Huang, P.I. Nagy, F.E. Williams, S.M. Peseckis, W.S. Messer, Roles of threonine 192 and asparagine 382 in agonist and antagonist interactions with M1 muscarinic receptors, Br. J. Pharmacol. 126 (1999) 735–745.
[45] S. Mordalski, T. Kosciolek, K. Kristiansen, I. Sylte, A.J. Bojarski, Protein binding site analysis by means of structural interaction fingerprint patterns, Bioorg. Med. Chem. Lett. 21 (2011) 6816–6819.
[46] S.G. Rasmussen, H.J. Choi, J.J. Fung, E. Pardon, P. Casarosa, P.S. Chae, B.T. Devree, D.M. Rosenbaum, F.S. Thian, T.S. Kobilka, A. Schnapp, I. Konetzki, R.K. Sunahara, S.H. Gellman, A. Pautsch, J. Steyaert, W.I. Weis, B.K. Kobilka, Structure of a nanobody-stabilized active state of the β_2 adrenoceptor, Nature 469 (2011) 175–180.
[47] T. Warne, R. Moukhametzianov, J.G. Baker, ′R. Nehme, P.C. Edwards, A.G. Leslie, G.F. Schertler, C.G. Tate, The structural basis for agonist and partial agonist action on a β_1-adrenergic receptor, Nature 469 (2011) 241–244.
[48] E. Yuriev, M. Agostino, P.A. Ramsland, Challenges and advances in computational docking: 2009 in review, J. Mol. Recognit. 24 (2011) 149–164.
[49] E. Yuriev, P.A. Ramsland, Latest developments in molecular docking: 2010–2011 in review, J. Mol. Recognit. 26 (2013) 215–239.
[50] Y. Miao, S.E. Nichols, P.M. Gasper, V.T. Metzger, J.A. McCammon, Activation and dynamic network of the M2 muscarinic receptor, Proc. Natl. Acad. Sci. U. S. A. (2013), http://dx.doi.org/10.1073/pnas.1309755110.